# Correlating GEDI and ALOS-2 Data for Biomass Assessment Over Singapore

Tze Yen CHUA[1*], Afiq Bin SULAIMAN[1], Ken Yoong LEE [2] and Soo Chin LIEW [3]

[1]Associate Scientist, [2]Research Scientist, [3]Principal Research Scientist,

Centre for Remote Imaging Sensing and Processing, National University of Singapore, Singapore

[*]tychua@nus.edu.sg

***Abstract:*** *Estimating forest biomass is critical for climate modelling and sustainable forest management. This study investigates the integration of GEDI LiDAR data and ALOS-2 PALSAR-2 data to enhance biomass assessment in Singapore. The GEDI provides high-resolution LiDAR data, offering detailed metrics such as above-ground biomass density and relative heights, while the ALOS-2's fully polarimetric synthetic aperture radar data offers valuable insights into vegetation biomass. Five ALOS-2 full-polarisation scenes were acquired between 28th May 2021 and 23rd April 2023 over Singapore. This study intended to correlate the GEDI-derived metrics with the ALOS-2 backscattering values, decomposed scattering powers, polarisation ratios, and radar vegetation index. The relationships between AGBD and the PolSAR parameters were examined using linear and exponential regression models. Preliminary findings revealed a relationship between both the GEDI's AGBD and RH metrics with the ALOS-2's parameter, particularly with HV sigma naught, volume scattering power, and radar vegetation index, achieving an $R^2$ of approximately 0.4 to 0.5 for some scenes. The application of linear and exponential regression models demonstrates SAR data's potential in biomass investigation and underscores the capability of integrating LiDAR and SAR data to enhance biomass estimation. This integrated approach offers a valuable tool for forest management and conservation efforts in tropical regions. The study emphasises the importance of synergistic data integration from diverse satellite sensors to improve the precision of biomass mapping, thereby contributing to global initiatives in monitoring and mitigating climate change impacts through enhanced forest carbon stock management.*

**Keywords:** Tropical forest, GEDI, Biomass, ALOS-2, L-band

## 1. Introduction

Singapore, a tropical city-state, presents unique challenges and opportunities for biomass assessment. Despite its relatively small size, Singapore hosts a range of forest types, including primary forests, secondary forests, and urban green spaces (Yee et al., 2011; Yee et al., 2019). These forests are crucial for the local and regional climate, supporting biodiversity and contributing significantly to carbon sequestration.

Singapore's forests mostly consist of tropical lowland rainforest, characterised by a variety of tree species adapted to the humid and warm climate. The primary forests, found mainly in protected areas such as the Bukit Timah Nature Reserve and the Central Catchment Nature Reserve (Noreen et al., 2013), are notable for their dense canopies and towering trees that can reach heights of up to 60 metres (Ho et al., 2019). In contrast, secondary forests and urban green spaces generally exhibit lower above-ground biomass density (AGBD) due to their younger age and more open canopy structures.

Given Singapore's dense urbanisation and limited land area, remote sensing technologies are crucial for monitoring and managing forest biomass. Satellite-based sensors such as GEDI (Global Ecosystem Dynamics Investigation) and ALOS-2 (Advanced Land Observing Satellite 2) provide valuable data for assessing forest structure and AGBD across different forest types. Integrating LiDAR (Light Detection and Ranging) and SAR (Synthetic Aperture Radar) data offers a promising approach to overcoming challenges associated with complex urban and tropical forest interfaces, potentially yielding more accurate and comprehensive AGBD estimates.

This study focuses on correlating GEDI-derived metrics such as canopy height (RH98) and AGBD with ALOS-2 backscattering values, decomposed scattering powers, polarisation ratios, and the radar vegetation index (RVI). The relationships between these GEDI-derived metrics and PolSAR (polarimetric SAR) parameters are examined using both linear and exponential regression models.

## 2. Materials and Methodology

### Study Area

The study area is situated in Singapore, encompassing a diverse range of natural and protected environments. This area includes the Central Catchment Nature Reserve, Bukit Timah Nature Reserve, Sungei Buloh Wetland Reserve, forested areas on smaller islands and various urban green spaces, including the Singapore Botanic Gardens, East Coast Park, and others. The spatial extent of the study area is illustrated in Figure 1. This figure provides a visual representation of the key regions within the study area and highlights the interconnected nature of the different reserves, parks, and forests. The data for this study was sourced from the Urban Redevelopment Authority (URA) and National Parks Board (NParks) supplying detailed information on nature reserves, parks, and land use.

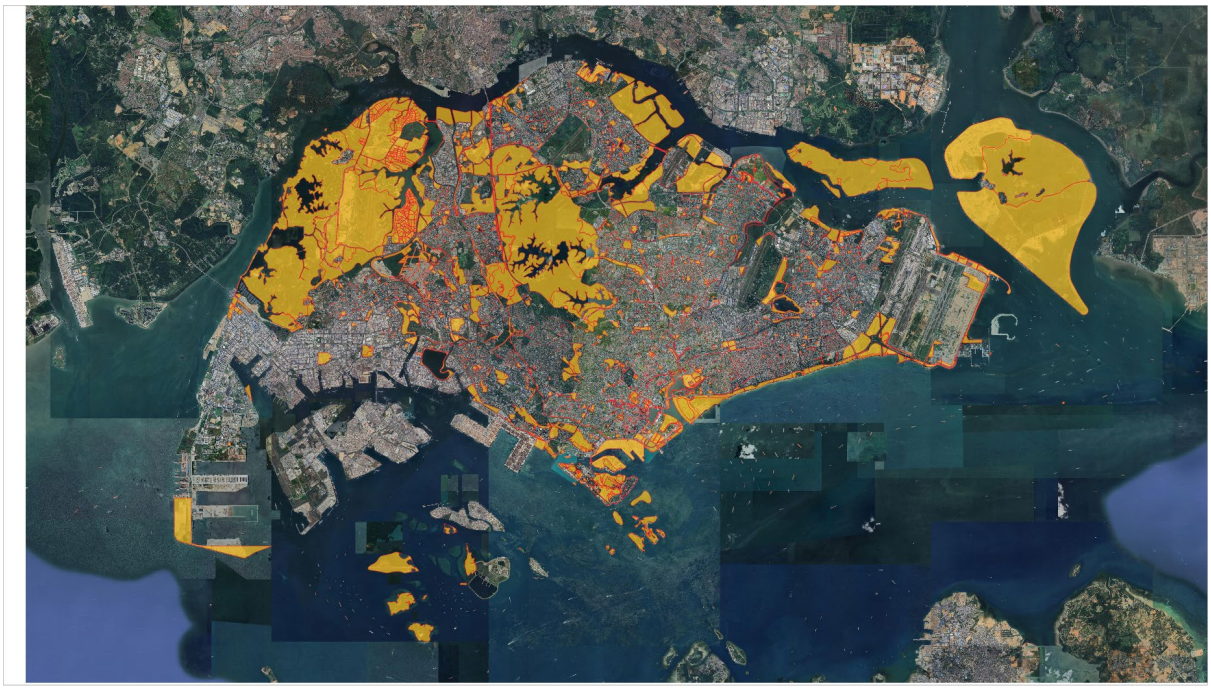

Figure 1: Study Area in Singapore highlighted by the yellow regions with red borders.

**GEDI Data**

The GEDI is a NASA mission designed to provide high resolution lidar data on the vertical structure of forests. GEDI data offers detailed information on forest canopy height, biomass, and other key forest metrics, which are crucial for understanding ecological dynamics and forest health. For this study, GEDI L2A Elevation and Height Metrics Data Global Footprint Level V002 (Dubayah et al., 2021) and GEDI L4A Footprint Level Aboveground Biomass Density, Version 2.1 (Dubayah et al., 2022) were utilised to extract estimates of canopy height (RH98) and AGBD on a footprint level (~25m diameter) within the study area as shown in Figure 2. The footprint level data contains a set of quality flags that allow filtering footprints with high geolocation uncertainty, poor signal quality, and shots affected by atmospheric noise and cloud cover (Dubayah et al., 2020) which we employed.

Figure 2: GEDI footprints and the corresponding data coverage for estimating AGBD and canopy height within the study area with darker greens showing higher AGBD. Footprints are not to scale.

**ALOS-2 PALSAR-2 Data**

In this study, we utilised five ALOS-2 PALSAR-2 quad-polarization single-look complex (SLC) datasets (Level 1.1). The details of these datasets are provided in Table 1, while Figure 3 illustrates their spatial coverage over the study area. The selection of ALOS-2 images was deliberately aligned with the temporal window of the GEDI data collection mission (2019 to 2023). This alignment was aimed at improving the consistency and comparability between the ALOS-2 and GEDI datasets for the analysis of tropical AGBD. Figure 4 shows selected scenes acquired over the study area.

Figure 3: ALOS-2 PALSAR-2 data coverages over the study area. Green and red coverages are over Singapore west and blue is over Singapore east with parts of Central Catchment Nature Reserve in the overlapping regions.

| **Scene ID** | ALOS2378673590-210528 | ALOS2456820017-221107 | ALOS2481660017-230424 |
|---|---|---|---|
| **Observation Date and Time** | 2021-05-28<br>04:50:36.292 UTC | 2022-11-07<br>17:15:25.427 UTC | 2023-04-24<br>17:15:24.102 UTC |
| **Radar Wavelength** | 24.2 cm | | |
| **Orbit Direction** | Descending | Ascending | |
| **Line Spacing** | 2.80 m | 2.79 m | |
| **Pixel Spacing** | 2.86 m | | |

Table 1a: Specifications of ALOS-2 PALSAR-2 data over Singapore west.

| **Scene ID** | ALOS2452680017-221010 | ALOS2479590017-230410 |
|---|---|---|
| **Observation Date and Time** | 2022-10-10<br><br>17:15:25.210 UTC | 2023-04-10<br><br>17:15:25.026 UTC |
| **Radar Wavelength** | 24.2 cm | |
| **Orbit Direction** | Ascending | |
| **Line Spacing** | 3.13 m | 3.13 m |
| **Pixel Spacing** | 2.86 m | 2.86 m |

Table 1b: Specifications of ALOS-2 PALSAR-2 data over Singapore east

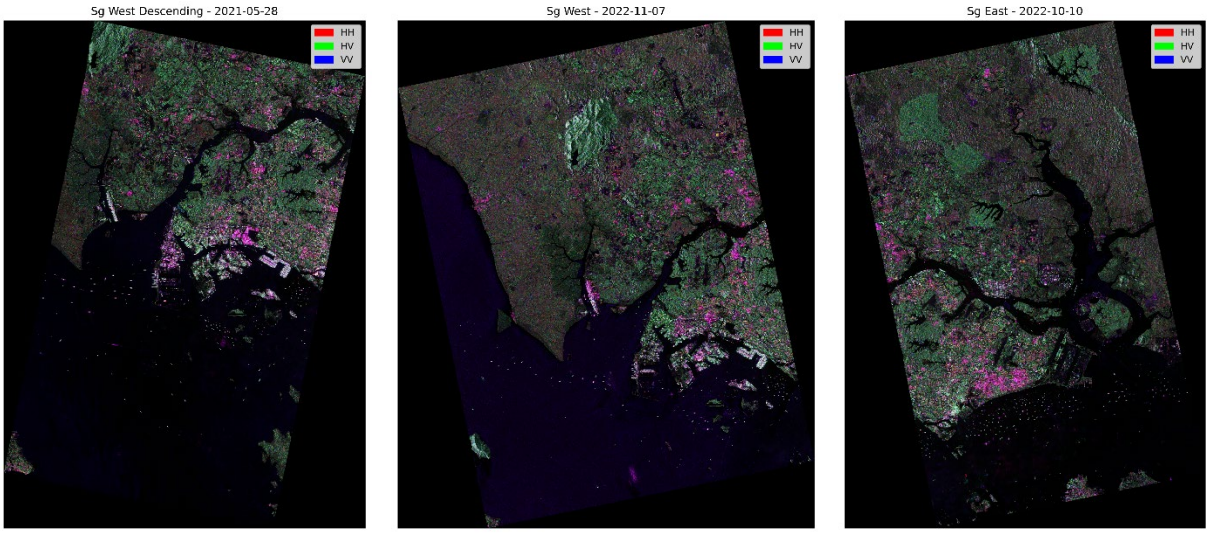


(a) (b) **(c)**

Figure 4: Selected ALOS-2 scenes acquired over Singapore west (a, b) and Singapore east (c).

The SLC data first undergoes radiometric calibration using

$$\sigma^0_{SLC} = 10 \cdot \log(I^2 + Q^2) + CF - A,$$

where $CF$ is -83.0 and $A$ is 32.0, as provided by Japanese Aerospace Exploration Agency (JAXA). Subsequently, the data undergoes multi-looking where radar returns are averaged over multiple looks in both the range and azimuth directions before applying the gravitation filter (Lee et al., 2021) to effectively suppress speckle noise. The decomposition of polarimetric radar data into meaningful scattering mechanisms (surface, double-bounce, volume and helical scattering) is achieved through the so-called iterative multistage polarimetric decomposition model (Lee et al., 2019). Finally, the images are orthorectified using backward geocoding with Copernicus 30m digital elevation model (Bayer et al., 1991).

Figure 5 shows selected scenes with the decomposed scattering powers acquired over the study area.

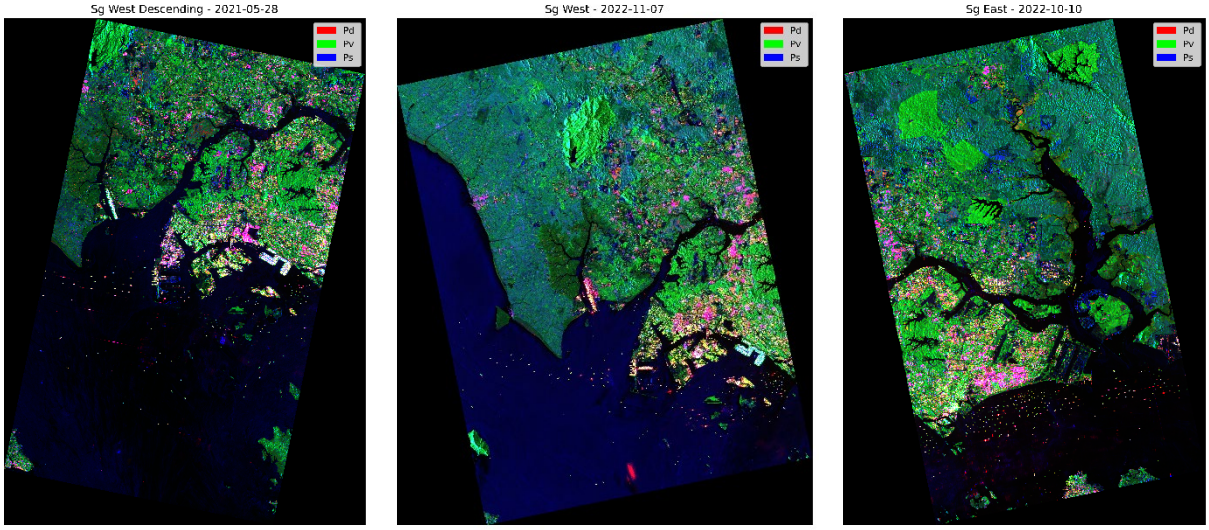


(a) (b) **(c)**

Figure 5: Decomposed scattering powers (Ps, Pd and Pv) of selected ALOS-2 scenes acquired over Singapore west (a, b) and Singapore east (c).

To assess the relationship between the GEDI-derived metrics and the backscattering values and decomposed scattering powers from ALOS-2, zonal statistics were used to extract mean backscattering values within geolocated GEDI footprints. A 25m diameter buffer is created around each GEDI footprints' locations. The diameter of 25m is chosen as it is the approximate diameter of the lidar footprint on the ground and corresponds to a specific location where AGBD and RH98 is measured. The mean backscattering values and decomposed scattering powers for each buffer zone were extracted within the 25m area surrounding each GEDI footprint. This process ensures that the backscattering values and scattering powers are proportionally representative of the area around each GEDI footprint. These mean values extracted from ALOS-2 were then matched with the corresponding GEDI AGBD and RH98 estimates. This integration facilitates the analysis of the relationship between AGBD, RH98 and backscattering intensities and scattering powers across different GEDI footprints over the study area. Additionally, the cross-polarisation ratios (CPR) (Henderson et al., 1998) and radar vegetation index (RVI) (Kim et al., 2009) were calculated and analysed as well:

$$\text{Cross} - \text{Polarisation Ratios: } \frac{\sigma_{HV}}{\sigma_{HH}} \text{ and } \frac{\sigma_{HV}}{\sigma_{VV}}$$

$$\text{Radar Vegetation Index: } \frac{8\sigma_{HV}}{\sigma_{HH} + 2\sigma_{HV} + \sigma_{VV}}$$

## 3. Results

To analyse the relationship between the canopy height (RH98) and AGBD from GEDI and the data from ALOS-2 images, scatter plots were created to visually inspect the correlation between these two datasets. The data also exhibit noticeable variability, implying that the relationship is not perfectly linear and that other factors may be influencing the correlation.

To further quantify the relationship, linear regression analysis was performed, and, where suitable, exponential regression analysis was also applied. These statistical analyses help in understanding both the strength and the nature of the association between GEDI-derived metrics and ALOS-2 data derived values, providing deeper insights into how well these datasets complement each other in estimating AGBD and canopy height in Singapore.

Figures 6 to 15 display the scatter plots of GEDI-derived RH98 and AGBD against mean ALOS-2 backscattering values (HH, HV, VV), decomposed scattering powers (Ps, Pd, Pv), cross-polarisation ratios and radar vegetation index. Each point on the plot represents a data pair from the GEDI and ALOS-2 datasets, with AGBD or RH98 on the y-axis and ALOS-2 data derived values on the x-axis. These plots show the general trends and distribution of data points, indicating how changes in ALOS-2 measurements relate to variations in RH98 and AGBD. A positive correlation is evident where higher backscattering values tend to correspond with increased biomass density or canopy height, suggesting that areas with greater backscattering generally have higher biomass.

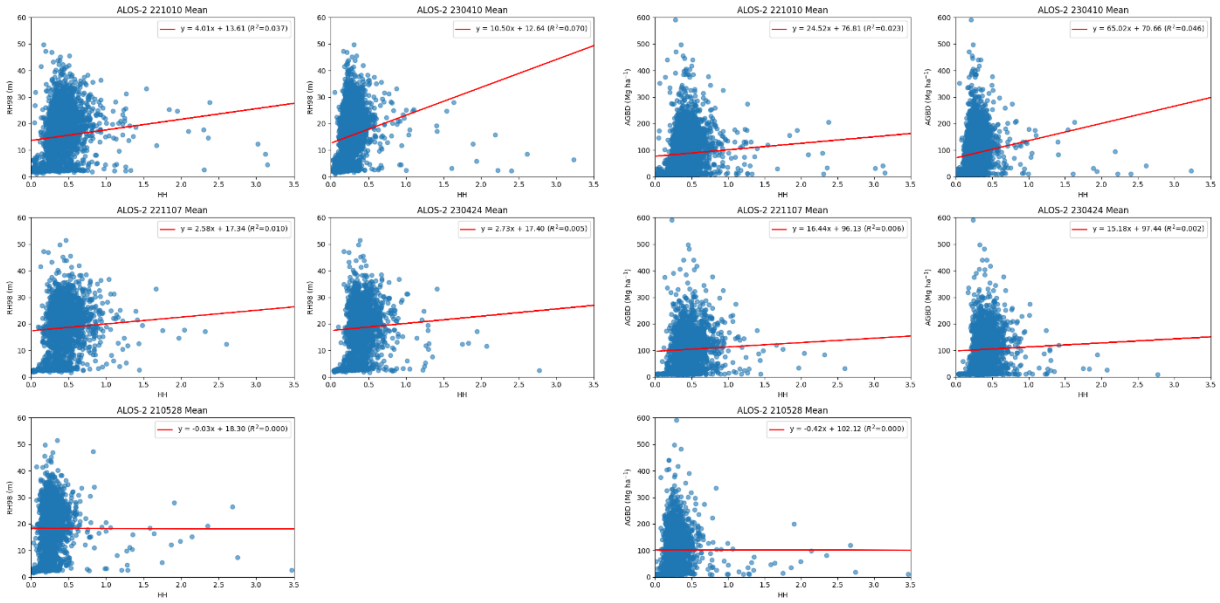


(a) (b)

Figure 6: Scatter plots showing the relationship between RH98 (a) and AGBD (b) with mean HH intensity from all five ALOS-2 Palsar-2 images, including the respective linear regression models.

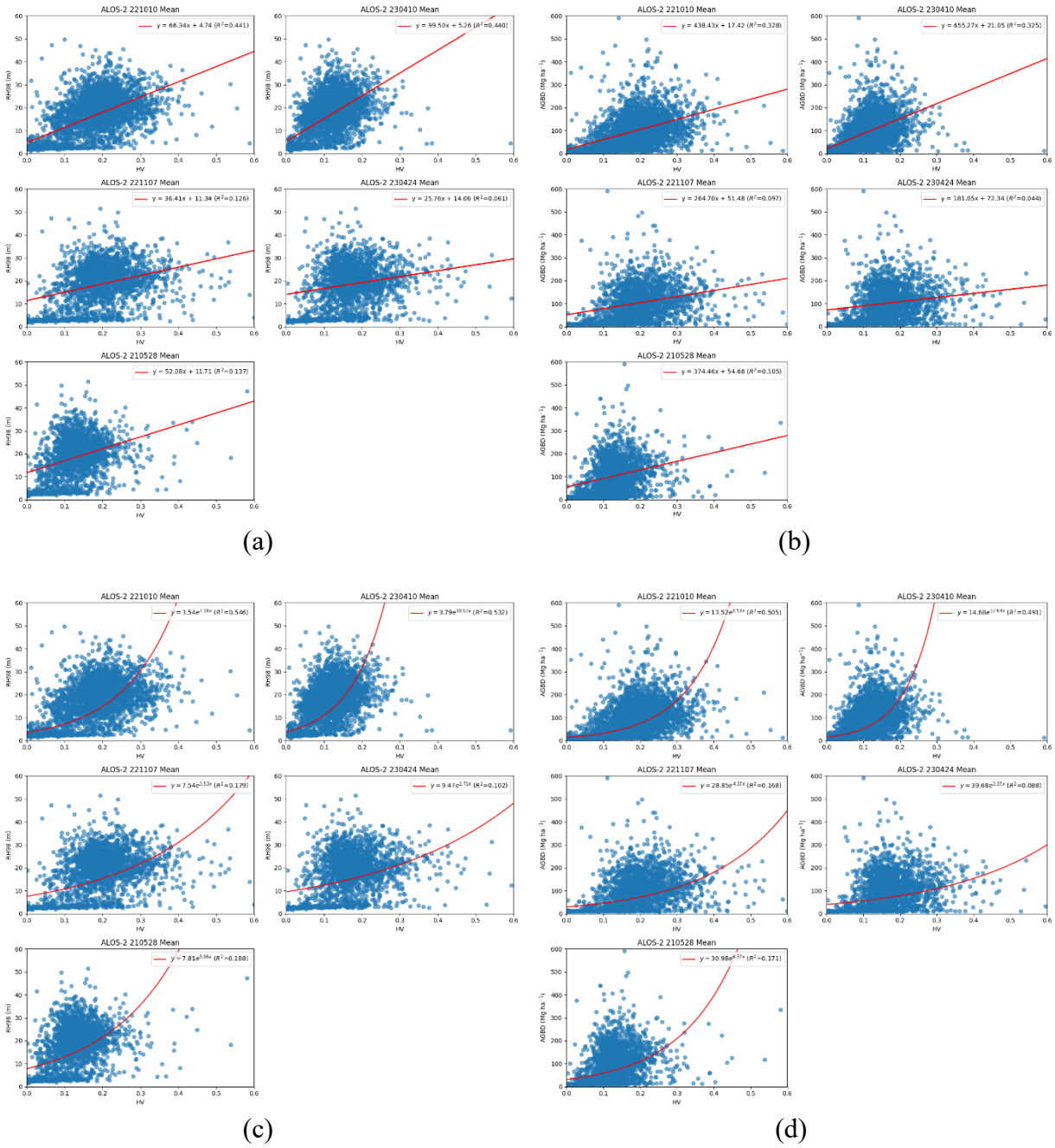


Figure 7: Scatter plots illustrating the relationship between RH98 (a, c) and AGBD (b, d) with mean HV intensity from all five ALOS-2 Palsar-2 images. Includes both linear (a, b) and exponential (c, d) regression models.

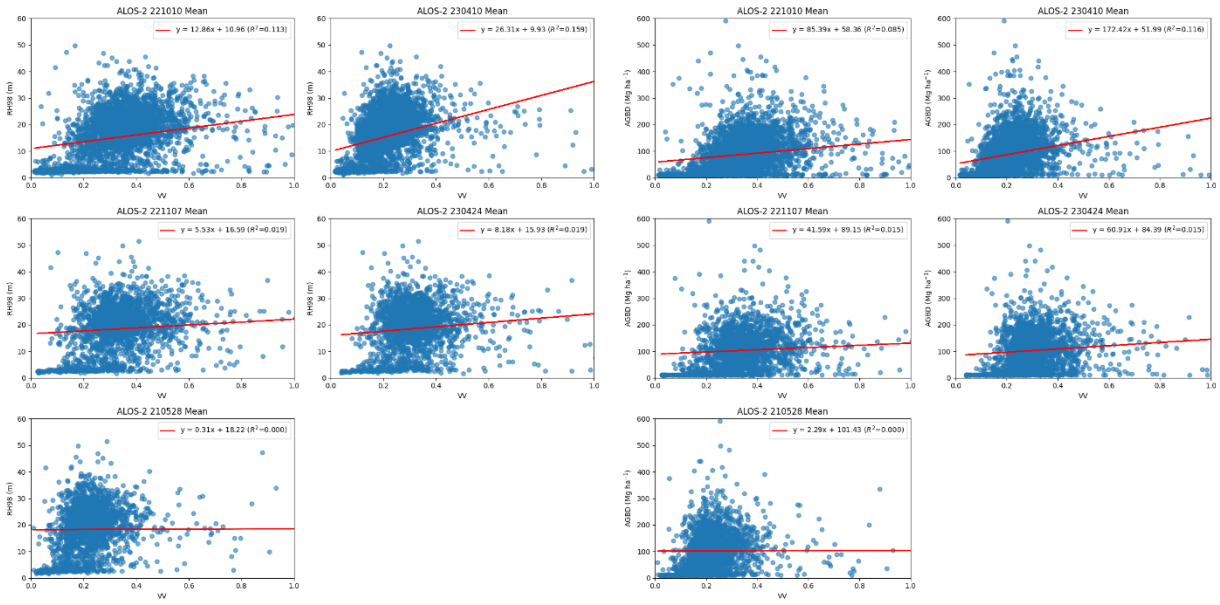


(a) (b)

Figure 8: Scatter plots showing the relationship between RH98 (a) and AGBD (b) with mean VV intensity from all five ALOS-2 Palsar-2 images, including the respective linear regression models.

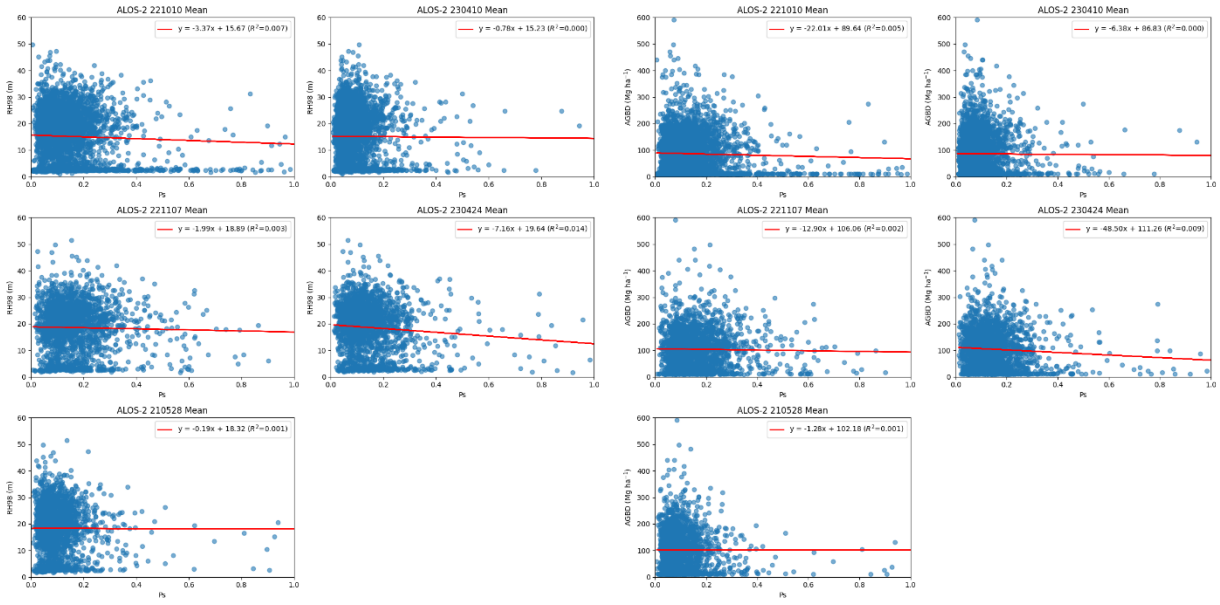


(a) (b)

Figure 9: Scatter plots showing the relationship between RH98 (a) and AGBD (b) with mean surface scattering power (Ps) from all five ALOS-2 Palsar-2 images, including the respective linear regression models.

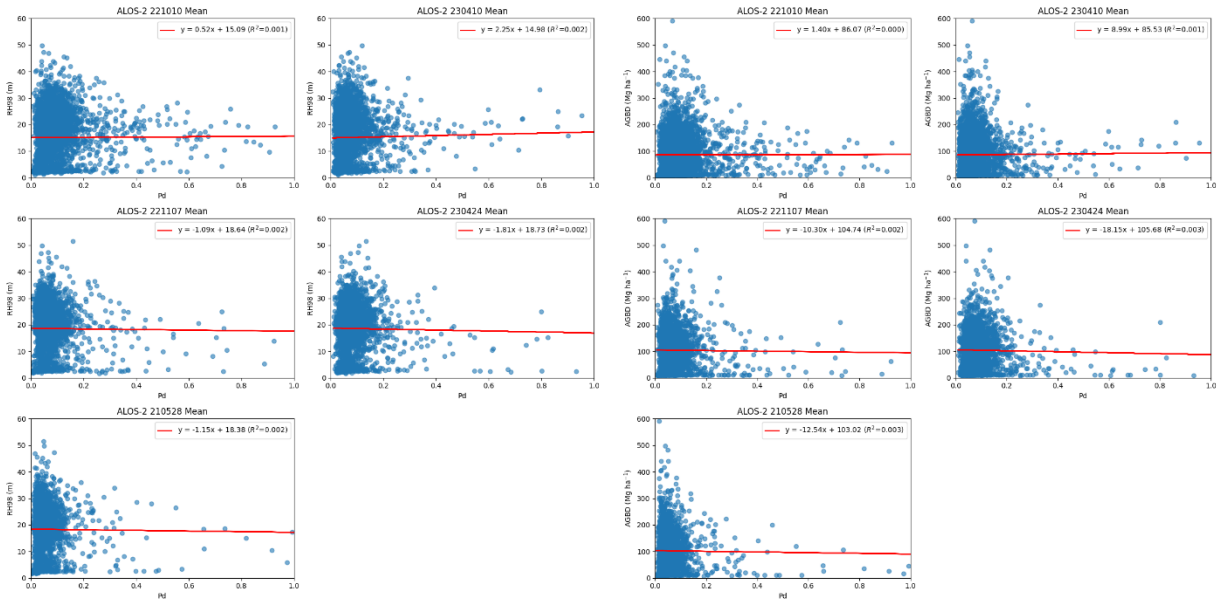


(a) (b)

Figure 10: Scatter plots showing the relationship between RH98 (a) and AGBD (b) with mean double-bounce scattering power (Pd) from all five ALOS-2 Palsar-2 images, including the respective linear regression models.

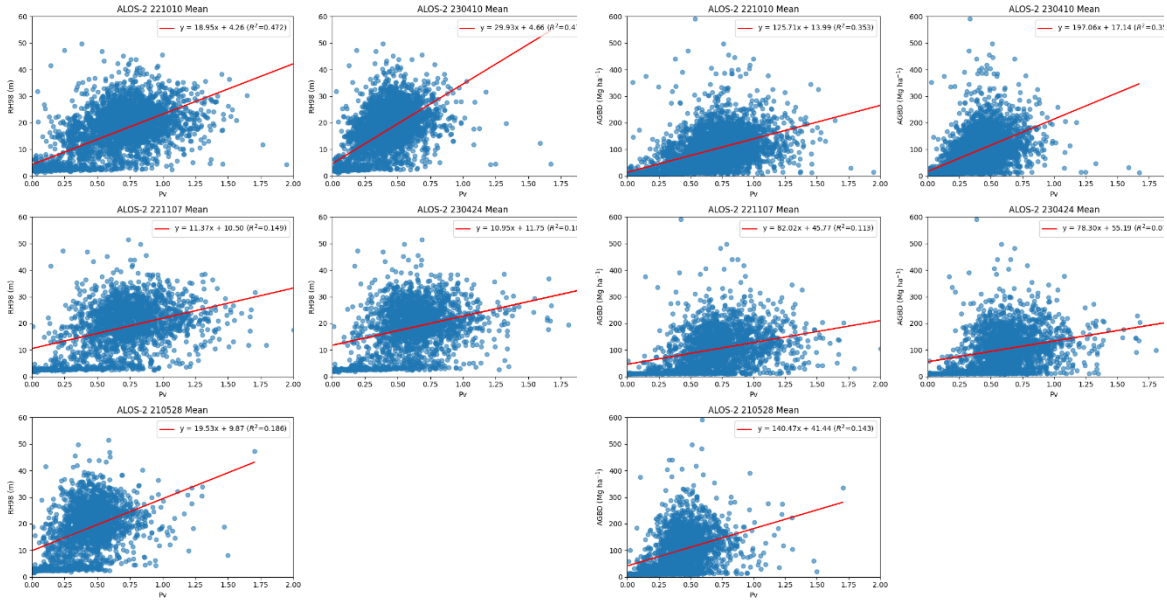


(a) (b)

Figure 11: Scatter plots showing the relationship between RH98 (a) and AGBD (b) with mean volume scattering power (Pv) from all five ALOS-2 Palsar-2 images, including the respective linear regression models.

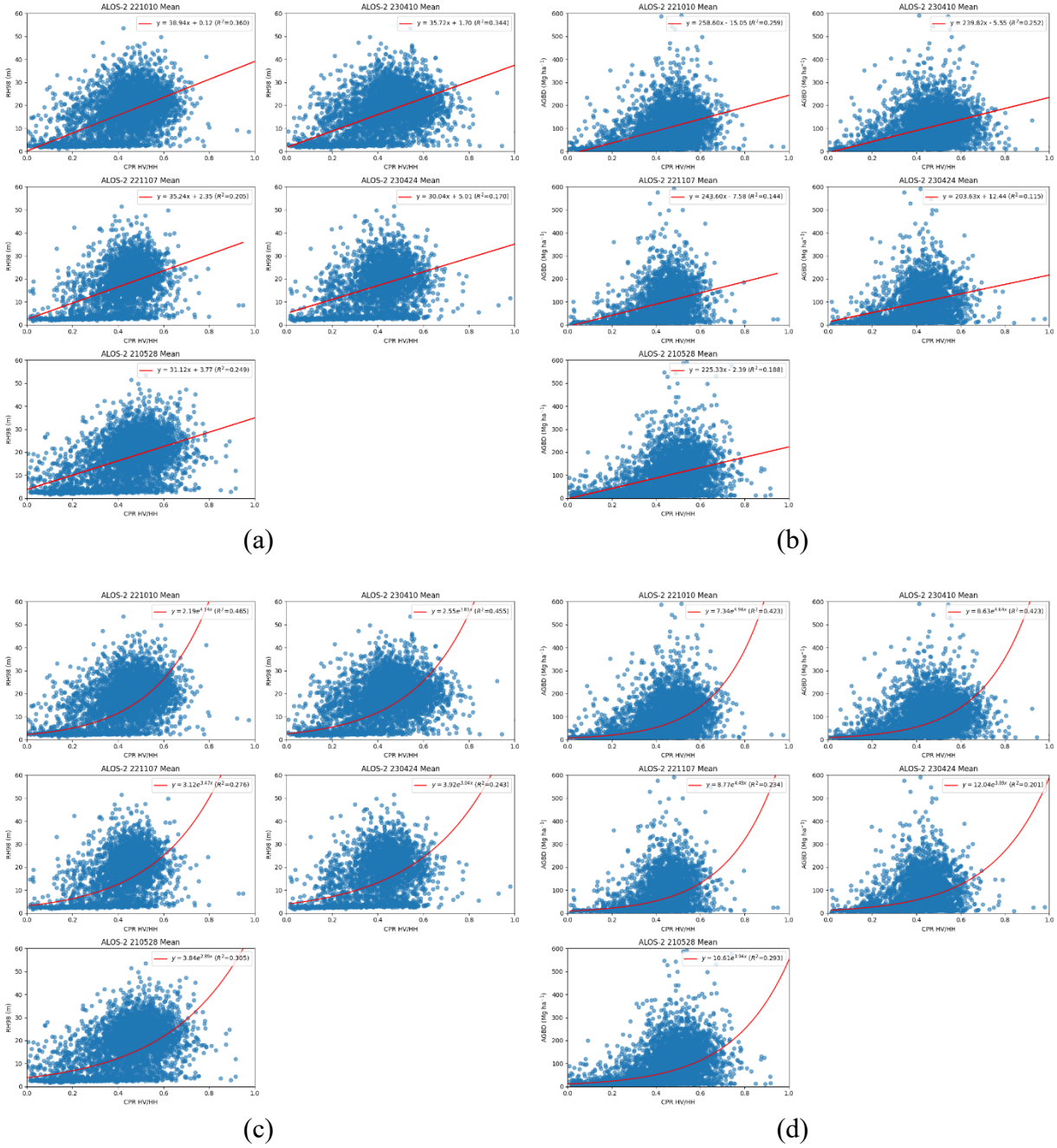


Figure 12: Scatter plots illustrating the relationship between RH98 (a, c) and AGBD (b, d) with mean cross-polarisation ratio $\left(\frac{\sigma_{HV}}{\sigma_{HH}}\right)$, from all five ALOS-2 Palsar-2 images. Includes both linear (a, b) and exponential (c, d) regression models.

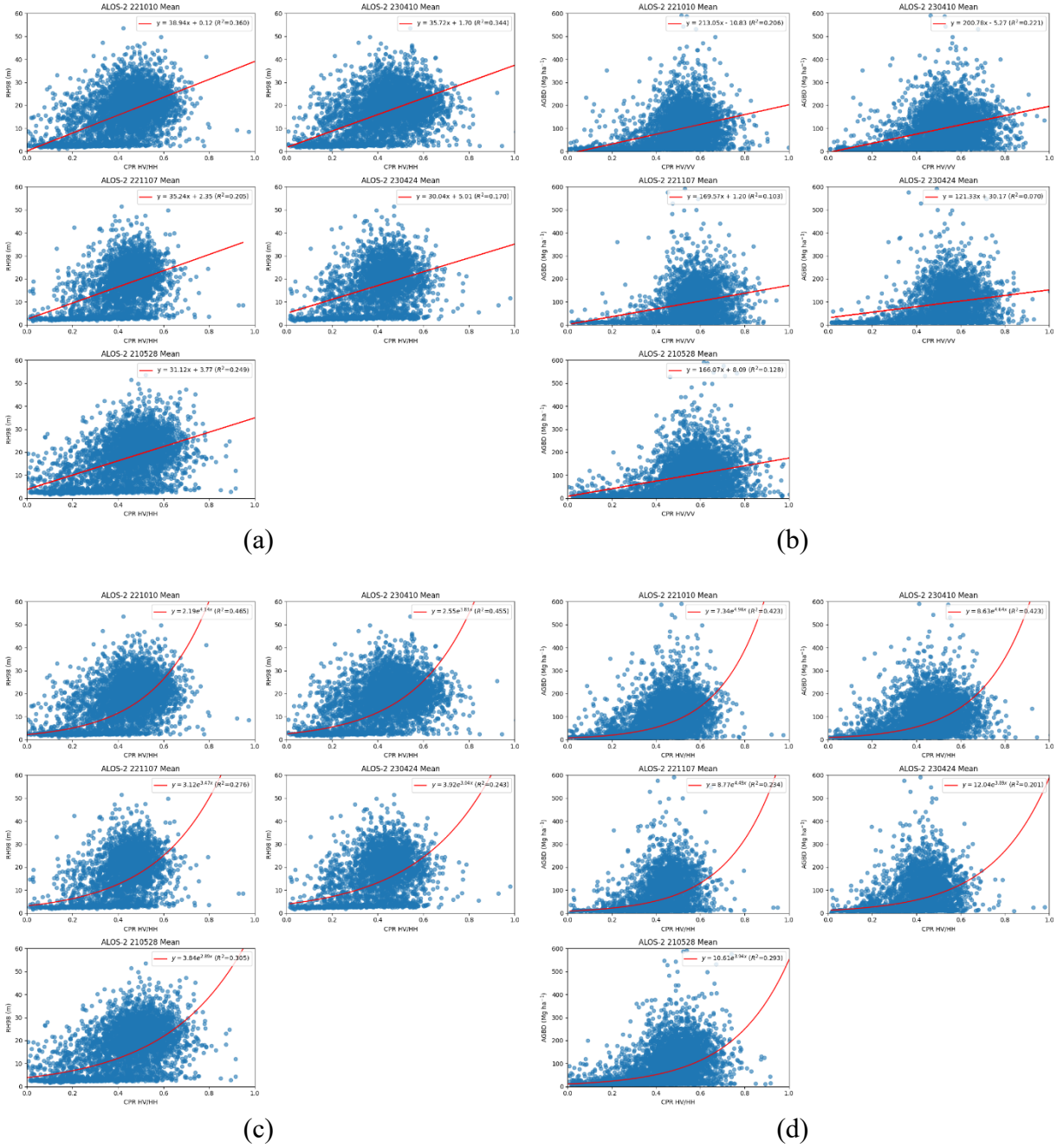


Figure 13: Scatter plots illustrating the relationship between RH98 (a, c) and AGBD (b, d) with mean cross-polarisation ratio $\left(\frac{\sigma_{HV}}{\sigma_{VV}}\right)$, from all five ALOS-2 Palsar-2 images. Includes both linear (a, b) and exponential (c, d) regression models.

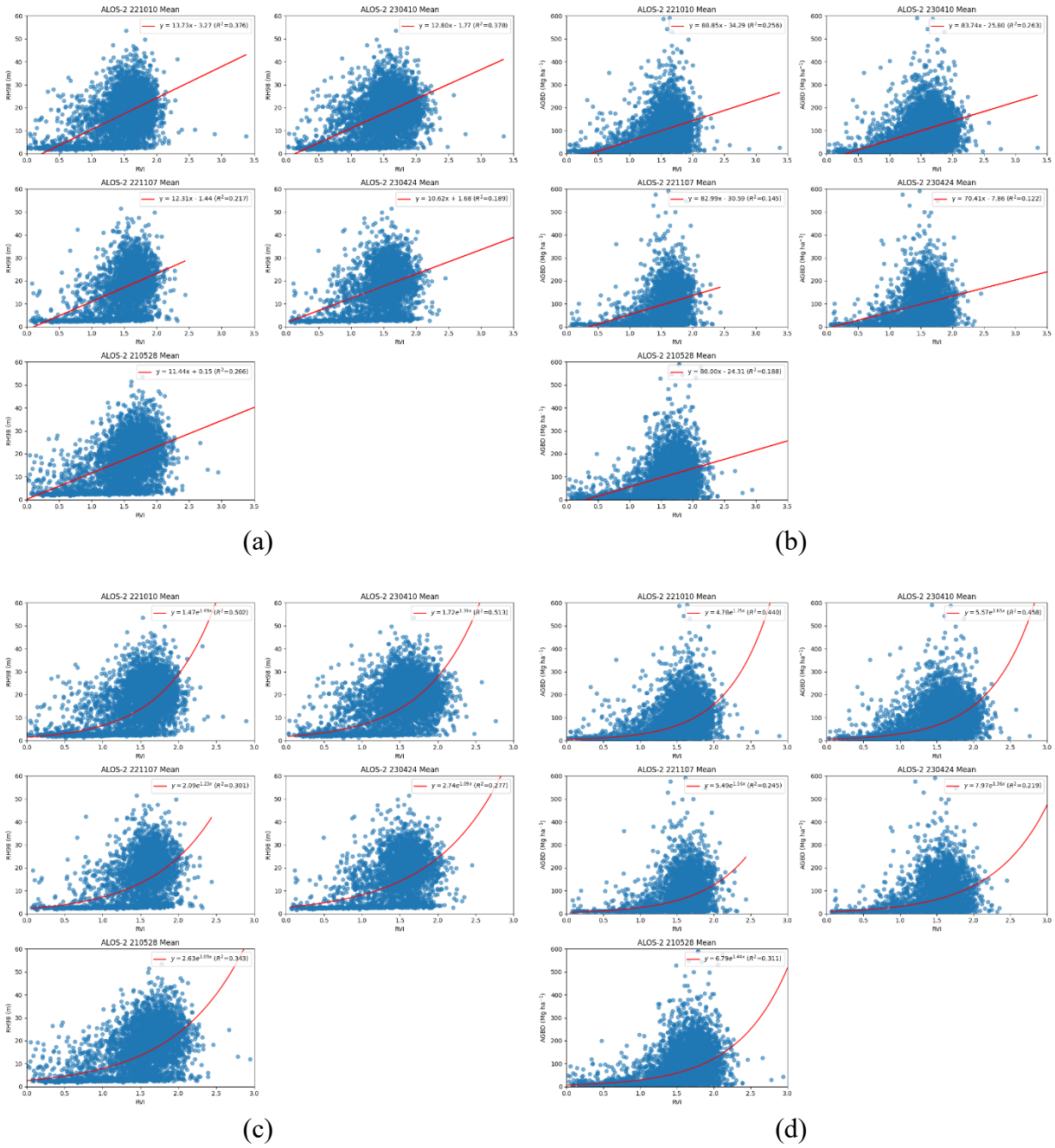


Figure 14: Scatter plots illustrating the relationship between RH98 (a, c) and AGBD (b, d) with mean radar vegetation index, from all five ALOS-2 Palsar-2 images. Includes both linear (a, b) and exponential (c, d) regression models.

## 4. Discussion and Conclusion

Among the backscattered intensities, the HV polarisation channel consistently exhibited the strongest $R^2$ values. For the two scenes from the eastern region of Singapore (ALOS2452680017-221010 and ALOS2479590017-230410), the $R^2$ values for HV backscattering were 0.441 and 0.440 for RH98, and 0.328 and 0.325 for AGBD, respectively. These results indicate that HV backscattering is particularly effective in capturing variations in canopy height and biomass density. Notably, the exponential regression models provided an even better fit, with $R^2$ values increasing to 0.546 and 0.523 for RH98 and 0.505 and 0.491

for AGBD in these scenes. This suggests that the relationship between HV backscattering and both RH98 and AGBD is non-linear, and the exponential model better represents the complexity of this relationship.

In terms of decomposed scattering powers, volume scattering power demonstrated the highest $R^2$ values among all scattering parameters. For the same two scenes in Singapore east, the $R^2$ values for volume scattering power were 0.472 and 0.475 for RH98, and 0.353 and 0.351 for AGBD. This indicates a robust correlation between volume scattering power and canopy height, reflecting its sensitivity to the structural attributes of vegetation. The comparatively lower $R^2$ values for AGBD suggest that while volume scattering power is a strong predictor for RH98, it is less effective in explaining variations in biomass density.

The analysis of cross-polarisations and the radar vegetation index revealed that their $R^2$ values were lower compared to the HV backscattering channel alone. Specifically, the $R^2$ values for both cross-polarisation ratios were consistently lower in both the eastern and western scenes, indicating that these ratios did not capture the variability in RH98 and AGBD as effectively as just HV backscattered intensities. Similarly, the radar vegetation index, which integrates multiple backscattering measurements to provide a composite indicator of vegetation, also showed weaker correlations compared to the HV polarisation channel alone.

This lower correlation with cross-polarisation ratios and the RVI suggests that while these parameters offer valuable supplementary information, they may not provide as clear or direct a measure of biomass density and canopy height as the HV backscattering channel. The weaker performance of these metrics could be due to the complexity of the relationships they represent or the inherent limitations in their ability to capture specific structural attributes relevant to biomass estimation.

In contrast, the three ALOS-2 scenes from the western region of Singapore exhibited much lower $R^2$ values relative to the eastern region. This stark difference suggests that the relationship between the remote sensing parameters and the GEDI-derived metrics is less pronounced or potentially influenced by different factors in the western scenes. Possible reasons for this variability could include differences in forest structure, land use, or other environmental variables that affect the backscattering and scattering power measurements. The lower $R^2$ values in these western scenes highlight the challenges of applying the same models and parameters across different regions with potentially distinct forest characteristics.

The findings underscore the importance of selecting the appropriate remote sensing parameters for accurate biomass estimation. HV backscattering and volume scattering power have shown promise in improving biomass estimates, particularly in the eastern scenes. However, the lower correlations observed with cross-polarisation ratios and the RVI indicate that these measures might not be as effective in isolation.

The variability across different scenes underscores the need for region-specific calibration of remote sensing models. Integrating multiple parameters and understanding regional differences are crucial for enhancing the accuracy of biomass assessments. Future research should focus on developing tailored models that account for regional variations and improve the overall precision of forest biomass estimation.

**Acknowledgements**

The authors would like to express their gratitude to the Office for Space Technology and Industry for awarding the incentive under the Space Technology Development Programme Grant.

**References**

Bayer, T., Winter, R., & Schreier, G. (1991). Terrain influences in SAR backscatter and attempts to their correction. *IEEE Transactions on Geoscience and Remote Sensing*, *29*(3), 451-462.

Dubayah, R., Blair, J. B., Goetz, S., Fatoyinbo, L., Hansen, M., Healey, S., ... & Silva, C. (2020). The Global Ecosystem Dynamics Investigation: High-resolution laser ranging of the Earth's forests and topography. *Science of Remote Sensing*, *1*, 100002.

Dubayah, R., Hofton, M., Blair, J., Armston, J., Tang, H., Luthcke, S. (2021). *GEDI L2A Elevation and Height Metrics Data Global Footprint Level V002* [Data set]. NASA EOSDIS Land Processes Distributed Active Archive Center. Accessed 2024-09-02 from https://doi.org/10.5067/GEDI/GEDI02_A.002

Dubayah, R.O., J. Armston, J.R. Kellner, L. Duncanson, S.P. Healey, P.L. Patterson, S. Hancock, H. Tang, J. Bruening, M.A. Hofton, J.B. Blair, and S.B. Luthcke. 2022. GEDI L4A Footprint Level Aboveground Biomass Density, Version 2.1. ORNL DAAC, Oak Ridge, Tennessee, USA. https://doi.org/10.3334/ORNLDAAC/2056

Henderson, F. M., & Lewis, A. J. (Eds.). (1998). *Principles and applications of imaging radar*. John Wiley & Sons.

Ho, B. C., Lua, H. K., Ibrahim, B., Yeo, R. S. W., Athen, P., Leong, P. K. F., ... & Middleton, D. J. (2019). The plant diversity in Bukit Timah Nature Reserve, Singapore. *The Gardens' Bulletin Singapore*, *71*, 41-144.

Japan Aerospace Exploration Agency (JAXA). (2016). *ALOS-2/PALSAR-2 Level 1.1/1.5/2.1/3.1 CEOS SAR product format description*. Retrieved from https://www.eorc.jaxa.jp/ALOS-2/en/doc/fdata/PALSAR-2_xx_Format_CEOS_E_f.pdf

Kim, Y., & van Zyl, J. J. (2009). A time-series approach to estimate soil moisture using polarimetric radar data. *IEEE Transactions on Geoscience and Remote Sensing*, *47*(8), 2519-2527.

Lee, K. Y., Hou, C., Liew, S. C., & Kwoh, L. K. (2019). Iterative multistage model-based decomposition for polarimetric synthetic aperture radar imagery. *2019 Asian Conference on Remote Sensing*, TuSS3-5.

Lee, K. Y., Hou, C., Liew, S. C., & Kwoh, L. K. (2021). Gravitation-Based Bilateral Filtering of ALOS-2 PALSAR-2 Polarimetric Data. *2021 IEEE International Geoscience and Remote Sensing Symposium*, 4747-4750.

Noreen, A. M., & Webb, E. L. (2013). High genetic diversity in a potentially vulnerable

tropical tree species despite extreme habitat loss. *PLoS One*, *8*(12), e82632.

Yee, A. T. K., Chong, K. Y., Seah, W. W., Lua, H. K., & Yang, S. (2019). Vegetation of Singapore. *Flora of Singapore*, *1*, 47-70.

Yee, A. T. K., Corlett, R. T., Liew, S. C., & Tan, H. T. (2011). The vegetation of Singapore - an updated map. *The Gardens' Bulletin Singapore*, *63*(1&2), 205-212.